



Cite this: *Chem. Commun.*, 2015, 51, 11413

Received 12th May 2015,  
Accepted 11th June 2015

DOI: 10.1039/c5cc03941j

www.rsc.org/chemcomm

## Unravelling the structure of the C<sub>60</sub> and *p*-Bu<sup>t</sup>-calix[8]arene complex

Xianjue Chen,<sup>a</sup> Ramiz A. Boulos,<sup>a</sup> Ashley D. Slattery,<sup>a</sup> Jerry L. Atwood<sup>b</sup> and Colin L. Raston<sup>\*a</sup>

The structure of the C<sub>60</sub> and *p*-Bu<sup>t</sup>-calix[8]arene complex has been reinvestigated, showing an unprecedented continuous layered tetragonal array of fullerenes encapsulated by calixarenes. Electron diffraction data revealed the tetragonal symmetry, with a stepped structure observed by AFM and SEM, and the thickness of the basal plane was measured by XRD, as 2 nm. The molecular simulated arrangement of fullerenes accounts for the ability to take up to ca. 11% of fullerenes C<sub>70</sub> in place of the smaller fullerene.

Supramolecular complexation of pristine fullerene C<sub>60</sub> involving inherently weak intermolecular forces offers scope for developing functional fullerene-based materials with controlled structures and tailored properties.<sup>1,2</sup> Macrocycles with electron-rich aromatic rings such as calix[*n*]arenes,<sup>3–8</sup> cyclotrimeratrylenes<sup>9,10</sup> and related molecules<sup>11–13</sup> can bind fullerenes, and have featured in gaining access to novel architectures. One of the earliest complexes of calixarenes with fullerenes is based on the readily available *p*-Bu<sup>t</sup>-calix[8]arene (Fig. 1a) which binds fullerene C<sub>60</sub> in toluene, forming a discrete 1 : 1 complex with some selectivity over other fullerenes.<sup>14,15</sup> Indeed this complexation is effective in separating and purifying fullerene C<sub>60</sub> from carbon soot.

Within the C<sub>60</sub>-*p*-Bu<sup>t</sup>-calix[8]arene complex the phenolic hydroxyl groups of the calixarene are expected to retain at least part of the cyclic hydrogen bonded array on binding fullerene C<sub>60</sub>, with some reorganisation of the aromatic groups in providing hydrophobic pockets with complementarity of curvature with that of the surface of C<sub>60</sub>, in optimizing  $\pi$ - $\pi$  interactions.<sup>5,16</sup> The complex is only sparingly soluble in toluene, but spontaneously decomposes in the presence of chlorinated solvents. While it is crystalline, the micaceous thin sheets have defied collecting suitable X-ray diffraction data for a single crystal structure determination. Based on the data available from over two decades, which included

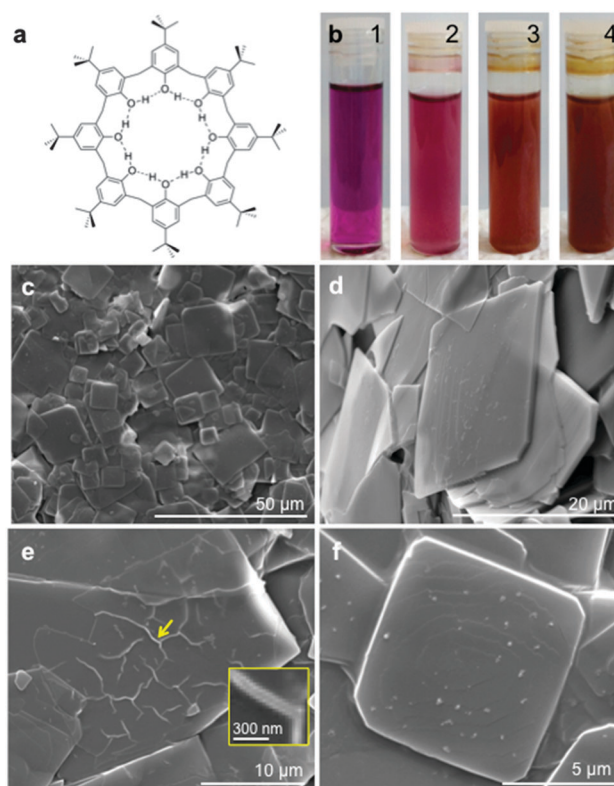


Fig. 1 (a) Chemdraw structure of *p*-Bu<sup>t</sup>-calix[8]arene. (b) The colour change in a toluene solution of C<sub>60</sub> induced by the addition of *p*-Bu<sup>t</sup>-calix[8]arene. (1: before the addition of *p*-Bu<sup>t</sup>-calix[8]arene; 2: mixing for 5 min; 3: mixing for 30 min; 4: mixing for 1 day) (c–f). SEM images of the C<sub>60</sub>-*p*-Bu<sup>t</sup>-calix[8]arene complex, showing square crystals ~5–30  $\mu$ m in size.

solid state NMR, UV-visible and FTIR spectroscopic data, analytical data (1 : 1 ratio of the two components) and molecular simulations, we proposed a triangular array of three fullerenes, with each of the three calixarenes in the double cone conformation spanning two fullerenes, positioned along the edges of the triangle.<sup>16</sup> With advances in transmission electron microscopy (TEM) and associated electron diffraction, scanning electron microscopy (SEM), Raman

<sup>a</sup> Centre for NanoScale Science and Technology, School of Chemical and Physical Sciences, Flinders University, Bedford Park, SA 5042, Australia.  
E-mail: colin.raston@flinders.edu.au; Tel: +61 88201 7958

<sup>b</sup> Department of Chemistry, University of Missouri, 601 South College Avenue, Columbia, Missouri 65211, USA



spectroscopy and atomic force microscopy (AFM), advanced molecular simulation coupled with the availability of greater computer power, we have reinvestigated this complex in an attempt to gain further insight into the nature of interplay of the components, with the results from the integrated approach consistent with an unprecedented layered tetragonal array of fullerenes.

The complex was prepared as a brown precipitate, following an adaption of the literature procedure,<sup>†14</sup> where by *p*-Bu<sup>t</sup>-calix[8]arene (176 mg) was added to a solution of C<sub>60</sub> (80 mg) dissolved in toluene (80 mL), with the colour of the solution changing gradually from magenta, to rose red (5 min), then brown (30 min), and ultimately dark brown (1 day), Fig. 1b. SEM images, Fig. 1c, established the precipitate present as square plates ~5–30 μm in cross section. An angular observation reveals the difference in thickness of the plates (Fig. 1d), generally <1 μm, and a few extremely thin layers can be seen, Fig. 1e, with the presence of wrinkles indicating an approximate thickness of the film, ~70 nm (inset). Fig. 1f reveals a typical spiral pattern on the surface of a plate, which is directed by screw dislocations that create steps from solute molecules for the nucleation and growth of layered crystals. The attachment of C<sub>60</sub> and *p*-Bu<sup>t</sup>-calix[8]arene molecules at the steps generates layers of terraces extending to the edge, forming layered square crystals.

In exploring the detailed growth mechanism of the complex, and in gaining further insight into its structure, AFM images were recorded on the precipitates that formed after five minutes and one day, Fig. 2a and b, respectively. The crystals formed after 5 minutes are square with round edges whereas after one day they are well defined, as thicker square plates. This reflects the different stages of nucleation and growth, with a layered structure initially formed. A similar layered growth feature is observed using SEM, Fig. 1f, as

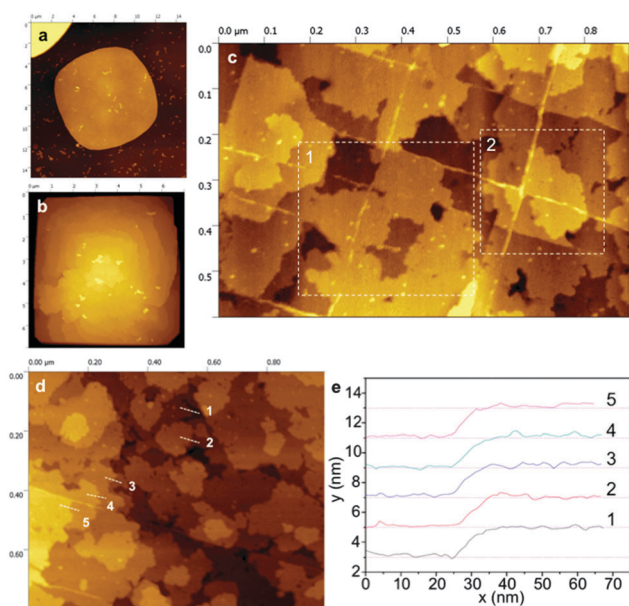


Fig. 2 AFM images of (a) a plate formed after 5 min (15 μm × 15 μm), and (b) a square plate formed after 1 day (7 μm × 7 μm). (c) Magnified image on the surface of the plate in (a), revealing the presence of islands for a layer growth (0.6 μm × 0.9 μm). (d) Magnified image on the surface of the plate in (a) (1 μm × 1 μm). (e) Height profiles following the lines indicated in (d), establishing a thickness of ~2 nm for each layer.

also evident using AFM, Fig. 2b. As the early stage of nucleation and growth is critical for investigating the molecular events, topographical studies on the surface of the crystal in Fig. 2a were undertaken, Fig. 2c and d, with the assumption that the nanoscale features at the surface may be 'frozen' upon a transfer to the substrate. The surface is relatively rough with many islands that are generated by the formation of 2D nuclei *via* a multinucleation multilayer growth, which occurs at high driving force conditions (high supersaturation). This is expected at the early stage of crystal growth where nucleation is more energetically favourable than the growth of steps to cover the whole surface. The spread and coalescence of these islands form layers, as in the indicated area (1) in Fig. 2c. A grid of fibres implies preferential direction that is intrinsically controlled by the tetragonal molecular structure of this complex (see below for details). The centre of the grid is expected to be the 2D nucleus, which grows rapidly towards four vertical crossing directions, and the solute molecules further attach to the grid at the corners or along the grid lines where a lower nucleation energy is required, as indicated in area (2), Fig. 2c. The height profiles for five ascending steps or islands on the surface in Fig. 2d are shown in Fig. 2e, establishing a consistent height of ~2 nm for each layer.

Raman spectra of the complex were acquired using a laser excitation wavelength of 785 nm and 50× objective. The precipitates were deposited onto a gold substrate, and an optical image of the square crystals is shown in Fig. 3. Raman spectra were selectively obtained on the crystal (blue cross), as well as on the gold substrate and the background (red cross). The corresponding Raman line for the complex shows typical prominent peaks for pristine C<sub>60</sub>, with the active fivefold degenerate H<sub>g</sub> and non-degenerate A<sub>g</sub> modes observed.<sup>17</sup> Compared with the spectrum for pristine C<sub>60</sub>, there is strong fluorescence background arising from the presence of C<sub>60</sub> in the complex. *p*-Bu<sup>t</sup>-calix[8]arene also has a well-defined Raman spectrum, which accounts for the appearance of a few low-frequency modes at 75.5 cm<sup>-1</sup>, 134.4 cm<sup>-1</sup>, and 166.2 cm<sup>-1</sup>, as

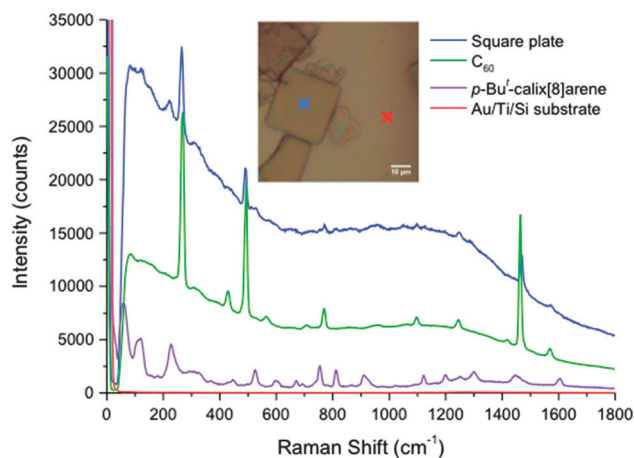


Fig. 3 Raman spectra for the square plate (blue line), Au/Ti/Si substrate (red line), and pristine C<sub>60</sub> (green line) and *p*-Bu<sup>t</sup>-calix[8]arene (magenta line), with the inset optical image showing the positions of the signals for the square plate and substrate.



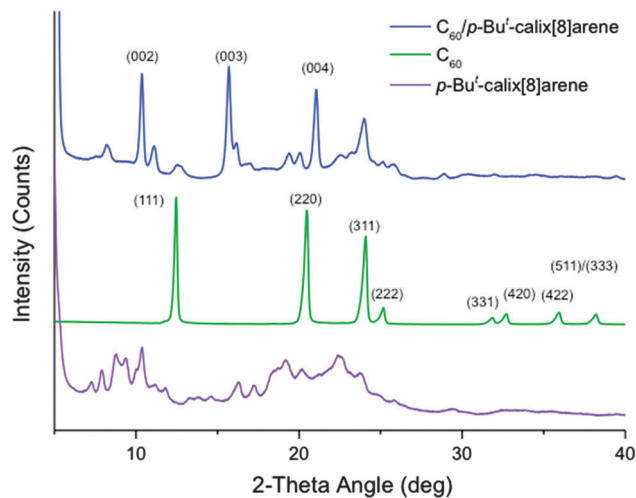


Fig. 4 The X-ray powder diffraction of the  $C_{60}$ - $p$ -Bu<sup>t</sup>-calix[8]arene complex.

well as the peaks appearing at  $236.7\text{ cm}^{-1}$  and  $536.9\text{ cm}^{-1}$  in the spectrum for the complex.

X-ray powder diffraction (XRD) data for the complex was recorded, Fig. 4, along with that for pristine  $C_{60}$  and  $p$ -Bu<sup>t</sup>-calix[8]arene powders. A direct comparison reveals that the structure of the complex is entirely different from both of the  $C_{60}$  and  $p$ -Bu<sup>t</sup>-calix[8]arene. The diffraction for pristine  $C_{60}$  shows a typical fcc crystal structure with eight feature reflections, as indexed. The XRD data indicates the basal plane  $d$ -spacing,  $\sim 1.95\text{ nm}$ , which is consistent with the thickness of the stepped structure in the AFM studies. Transmission electron microscopy (TEM) also showed the presence of square prismatic crystals, Fig. 5, although they were sensitive to the electron beam with cracks appearing during the characterisation and the disappearance of the electron diffraction pattern after a few seconds of exposure. A careful and rapid operation managed to preserve a selected area electron diffraction pattern, Fig. 5b, which revealed a unique pattern consistent with a tetragonal structure. This pattern suggests an  $x$ - $y$  dimension of  $\sim 2.8\text{ nm}$  which is an important consideration in developing a model using molecular simulations (see below).

Molecular simulations were carried out to develop a model for the structure of the complex between fullerene  $C_{60}$  and  $p$ -Bu<sup>t</sup>-calix[8]arene which incorporates tetragonal symmetry,

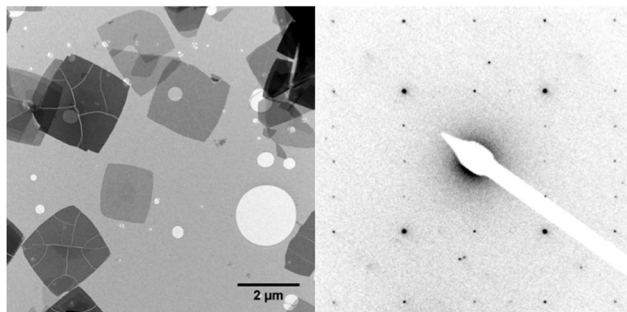


Fig. 5 TEM image of the as-prepared  $C_{60}/p$ -Bu<sup>t</sup>-calix[8]arene crystals, and a selected area electron diffraction pattern from a crystal, showing a unique pattern for tetragonal symmetry.

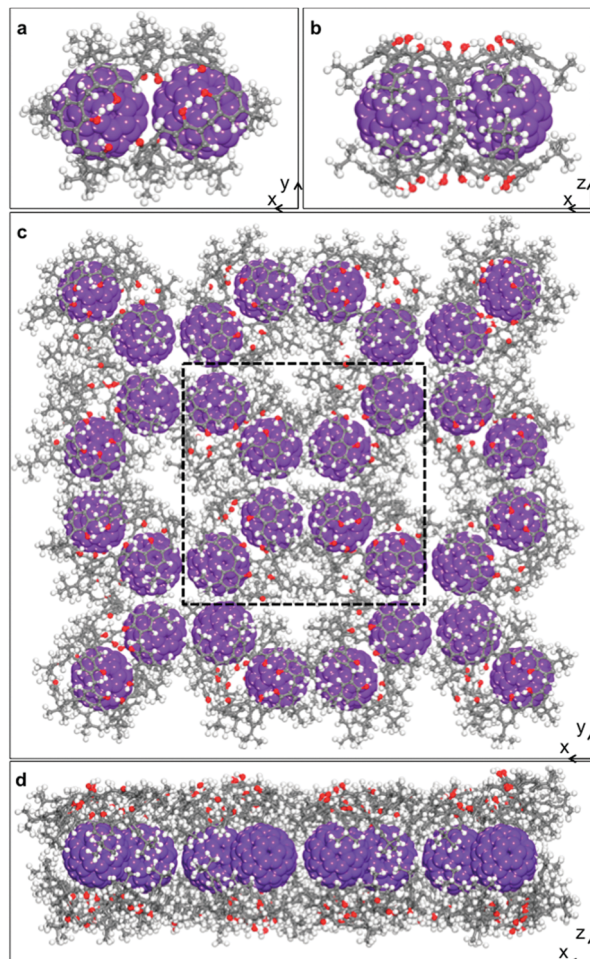


Fig. 6 Molecular simulations of the structure of the  $C_{60}$ - $p$ -Bu<sup>t</sup>-calix[8]arene complex (see text for details).

the spacing in the basal plane, and earlier data, with the results shown in Fig. 6. The minimised model has a pair of  $C_{60}$  molecules at the van der Waals limit ( $\sim 1\text{ nm}$ ), shrouded by two  $p$ -Bu<sup>t</sup>-calix[8]arenes in a double cone conformation, above and below the basal plane, Fig. 6a and b. These calixarenes effectively block any association with other fullerenes at right angles to the vector between the pair of fullerenes, but with the terminal surface area of these fullerenes available for interaction with other fullerenes. Contact of each fullerene in this pair of fullerenes with two other pairs of fullerenes builds up a tight tetragonal packing of pairs of fullerenes, as a unit cell indicated in the dashed square in Fig. 6c. This arrangement of fullerenes is without compromising on maximising the contact surface area of each calixarene with a pair of fullerenes. The model is consistent with the established 1:1 ratio of the two components, and that two  $p$ -tert-butylphenol groups for each calixarene are distinct from the other six in lying astride two  $C_{60}$  molecules. The thickness of each layer, comprised of a layer of  $C_{60}$  molecules capped either side by a layer of calixarenes, is  $\sim 2\text{ nm}$  (Fig. 6d), which is in accord with the above results from the AFM and XRD. The model is also consistent with the electron diffraction pattern, with the  $x$ - $y$  dimension of the unit



cell in this model  $\sim 2.8$  nm. Thus while the calixarenes make a number of fullerene contacts, as is common in such host-guest complexes with fullerenes, the expected hexagonal closed packed array of fullerenes in a single sheet is disrupted. Indeed the arrangement of the fullerenes in the basal plane effectively creates 'holes' which are occupied by geometrically opposed substituted phenyl rings within each calixarene, with each hole occupied by four such rings from four different calixarenes, in a tetragonal array. This more open arrangement of fullerenes relative to hexagonal close packing in 2D sheets is also consistent with the fullerenes being less confined rotationally, which is in turn consistent with the solid state NMR results, where free rotation of the fullerene in the complex occurs at room temperature. Such cavities may offer spatial flexibility in the structure for the replacement of some of the  $C_{60}$  molecules by  $C_{70}$  (up to 11% established experimentally).<sup>14</sup> If the principle axis of  $C_{70}$  is in the plane of the fullerenes, then there would be no perturbations to the thickness of the composite layers.

We have established a unique tetragonal structure of the complex between  $C_{60}$  and *p*-Bu<sup>t</sup>-calix[8]arene using a repertoire of contemporary characterization techniques (SEM, TEM, AFM, XRD and Raman spectroscopy), coupled with advanced molecular simulations. Importantly the electron diffraction data revealed tetragonal symmetry, which along with the stepped structure (AFM) and the thickness of the basal plane (XRD), provides crucial data in unravelling the nature of the structure. In addition, this less restricted arrangement of fullerenes accounts for the ability to take up to ca. 11% of fullerenes  $C_{70}$  in place of fullerene  $C_{60}$  while still retaining the same structure.<sup>14</sup> The earlier proposed structure based on a triangular array of fullerenes was modelled for including a  $C_{70}$  molecule with two  $C_{60}$  molecules, but this significantly distorts the structure.

We gratefully acknowledge the support of this work by the Australian Research Council and The Government of South Australia. The authors acknowledge the facilities, and the scientific and technical assistance on the AFM and Raman spectrometry studies, supported by the Australian Microscopy & Microanalysis Research Facility (AMMRF) and Australian National Fabrication Facility (ANFF) at Flinders University. TEM analysis was carried out using the facilities in Adelaide Microscopy at The University of Adelaide. X-ray diffraction was performed using the facility in The Bragg Crystallography Facility at The University of Adelaide. The authors also would like to thank Peter G. Self for valuable discussions.

## Notes and references

† *Methods summary*: pristine fullerene  $C_{60}$  (99685-96-8, 99+%, BuckyUSA) and toluene (1.08327.4000, 99.9%, Merck Millipore) were used as purchased. *p*-But-calix[8]arene was synthesised following the established protocol in the previous report.<sup>14</sup> SEM imaging was performed

on the FEI Quanta 450 High Resolution Field Emission SEM, with a voltage of 10 kV, and working distance of 10 mm. For TEM, toluene solutions with precipitates were drop-cast onto 200 mesh holey carbon copper grids (#2450-AB, SPI Supplies), and dried in air. FEI Tecnai G2 Spirit TEM equipped with a FEG LaB6 emitter operating at a voltage of 120 kV was used for acquiring the TEM and SAED data. The imaging was done *via* an in-column Olympus-SIS Veleta CCD camera. Image J software was used for processing all the TEM images. AFM images were acquired in air using a Bruker Dimension FastScan AFM with Nanoscope V controller, operating in PeakForce Tapping mode. The solutions were drop-cast onto freshly cleaved mica substrates and dried in air prior to AFM analysis. Bruker ScanAsyst Air probes with a nominal tip radius of 2 nm and nominal spring constant of  $0.4 \text{ N m}^{-1}$  were used. Imaging parameters including set-point, scan rate (1–2 Hz) and feedback gains were adjusted to optimize image quality and minimize imaging force. The AFM scanner was calibrated in the *x*, *y* and *z* directions using silicon calibration grids (Bruker model numbers PG: 1  $\mu\text{m}$  pitch, 110 nm depth and VGRP: 10  $\mu\text{m}$  pitch, 180 nm depth). Images were analysed using the Gwyddion free SPM software (version 2.38). Raman spectra were recorded using a Horiba Xplora Raman system with 785 nm excitation wavelength. The substrate was prepared by sputter coating 20 nm Ti and then 100 nm Au layers onto a silicon substrate to completely block the silicon background signal. XRD spectra were acquired using a Bruker D4 Endeavour 66 sample powder X-ray diffractometer (Co source). The Discover Module in Materials studio V5.5.3 was used for the energy minimisations of the complex. A tetragonal geometry of calixarene and  $C_{60}$  was generated using the visualiser module of Materials Studio. The Steepest descent algorithm was used for minimisation with a convergence tolerance of  $0.001 \text{ kcal mol}^{-1}$  for energy and  $0.5 \text{ kcal mol}^{-1} \text{ \AA}^{-2}$  for force with 500 000 iterations. The cell parameters were unfixed allowing optimisation to dictate the size of the system. The Drieding forcefield was used to incorporate hydrogen bonding on the lower rim of the calixarenes.

- 1 S. S. Babu, H. MöHwald and T. Nakanishi, *Chem. Soc. Rev.*, 2010, **39**, 4021.
- 2 T. Aida and K. Tashiro, *Chem. Soc. Rev.*, 2007, **36**, 189.
- 3 M. Makha, A. Purich, C. L. Raston and A. N. Sobolev, *Eur. J. Inorg. Chem.*, 2006, 507.
- 4 D. Sun and C. A. Reed, *Chem. Commun.*, 2000, 2391.
- 5 J. L. Atwood, L. J. Barbour, M. W. Heaven and C. L. Raston, *Angew. Chem., Int. Ed.*, 2003, **42**, 3254.
- 6 J. L. Atwood, L. J. Barbour, C. L. Raston and I. B. N. Sudria, *Angew. Chem., Int. Ed.*, 1998, **37**, 891.
- 7 J. L. Atwood, L. J. Barbour, P. J. Nichols, C. L. Raston and C. A. Sandoval, *Chem. – Eur. J.*, 1999, **5**, 990.
- 8 L. J. Hubble and C. L. Raston, *Chem. – Eur. J.*, 2007, **13**, 6755.
- 9 J. W. Steed, P. C. Junk and J. L. Atwood, *J. Am. Chem. Soc.*, 1994, **116**, 10346.
- 10 J. L. Atwood, M. J. Barnes, M. G. Gardiner and C. L. Raston, *Chem. Commun.*, 1996, 1449.
- 11 M. J. Hardie and C. L. Raston, *Chem. Commun.*, 1999, 1153.
- 12 M. Norret, M. Makha, A. N. Sobolev and C. L. Raston, *New J. Chem.*, 2008, **32**, 808.
- 13 M. Makha, J. L. Scott, C. R. Strauss, A. N. Sobolev and C. L. Raston, *Cryst. Growth Des.*, 2009, **9**, 483.
- 14 J. L. Atwood, G. A. Koutsantonis and C. L. Raston, *Nature*, 1994, **368**, 229.
- 15 T. Suzuki, K. Nakashima and S. Shinkai, *Chem. Lett.*, 1994, 699.
- 16 C. L. Raston, J. L. Atwood, P. J. Nichols and I. B. N. Sudria, *Chem. Commun.*, 1996, 2615.
- 17 J. Winter and H. Kuzmany, *J. Raman Spectrosc.*, 1996, **27**, 373.

